Spatiotemporal Variability of ENSO and SST Teleconnections to Summer Drought over the United States during the Twentieth Century

BALAJI RAJAGOPALAN AND EDWARD COOK

Lamont-Doherty Earth Observatory, Columbia University, Palisades, New York

UPMANU LALL

Utah Water Research Laboratory, Utah State University, Logan, Utah

BONNIE K. RAY

New Jersey Institute of Technology, Newark, New Jersey

(Manuscript received 23 July 1999, in final form 12 January 2000)

ABSTRACT

Presented are investigations into the spatial structure of teleconnections between both the winter El Niño–Southern Oscillation (ENSO) and global sea surface temperatures (SSTs), and a measure of continental U.S. summer drought during the twentieth century. Potential nonlinearities and nonstationarities in the relationships are noted. During the first three decades of this century, summer drought teleconnections in response to SST patterns linked to ENSO are found to be strongest in the southern regions of Texas, with extensions into regions of the Midwest. From the 1930s through the 1950s, the drought teleconnection pattern is found to extend into southern Arizona. The most recent three decades show weak teleconnections between summer drought over southern Texas and Arizona, and winter SSTs, which is consistent with previous findings. Instead, the response to Pacific SSTs shows a clear shift to the western United States and southern regions of California. These epochal variations are consistent with epochal variations observed in ENSO and other low-frequency climate indicators. This changing teleconnection response complicates statistical forecasting of drought.

1. Introduction

Understanding interannual to interdecadal variations in continental drought is important for improved water resource planning and management. The 1988 drought and accompanying heat waves over the midwestern United States caused around $39 billion in damages and contributed to increased heat-related mortality rates (Riebsame et al. 1991; Trenberth and Branstator 1992). Water rights allocations and reservoir operating rules are predicated on long-term assessments of drought frequency, and seasonal to interannual forecasts of seasonal drought are of interest for crop insurance, reservoir operation, and disaster planning.

Associations of North American hydrologic drought with the El Niño–Southern Oscillation (ENSO) have been identified in previous studies (Piechota and Dracup 1996; Trenberth and Branstator 1992; Cole and Cook 1998). Other researchers (Ropelewski and Halpert 1986, 1989; Halpert and Ropelewski 1992; Kiladis and Diaz 1989) have also identified strong relationships between ENSO and seasonal mean anomalies in U.S. temperatures and precipitation, which are key factors in the initiation of drought. ENSO is understood as an interannual, quasiperiodic, coupled mode of the tropical ocean–atmosphere system, with worldwide hydroclimatic teleconnections (Battisti and Sarachik 1995). The strength, duration, and frequency of the El Niño and La Niña events, which comprise the two phases of ENSO, have varied significantly over the current century (Trenberth and Hoar 1996, 1997; Rajagopalan et al. 1997; Kestin et al. 1998). Indeed, significant variations in ENSO are noted in a 10 000-yr integration of the Cane–Zebiak ENSO model (Cane et al. 1995) under a stationary climate scenario. Corresponding changes in the nonlinear response of the tropical and extratropical atmosphere (Hoerling et al. 1997) and in the North American climate (Hoerling and Kumar 1997) have also been noted from analyses of data obtained from both observational and climate model studies.

Decadal variations in ENSO teleconnections to con-

Corresponding author address: Balaji Rajagopalan, Dept. of Civil, Env. and Arch. Engineering, University of Colorado, ECOT-541, Campus Box 428, Boulder, CO 80309-0428.
E-mail: balajir@colorado.edu

tinental temperature, precipitation, stream flow, and drought indices around the globe have also been noted by many. In particular, Power et al. (1999) noted decadal variability in ENSO teleconnections to Australian climate and suggested that it might be due to interdecadal Pacific oscillation; Krishna Kumar et al. (1999a,b) noted decadal changes in the Indian summer monsoon–ENSO association; Rodo et al. (1997) saw changes in ENSO and North Atlantic Oscillation (NAO) teleconnections to southern Europe precipitation; and Price et al. (1998) found an increasing association of northern Israel precipitation to ENSO in the recent decades. Temporal variations in ENSO teleconnections to U.S. climate have also been reported; McCabe and Dettinger (1998), Dettinger et al. (1995, 1998), and Cayan et al. (1998) found decadal variability in ENSO teleconnections to western U.S. precipitation, and Cole and Cook (1998) noted changes in the spatiotemporal variability in U.S. summer Palmer Drought Severity Index (PDSI), while Dai et al. (1998) found decadal variations in the areas of severe drought over the globe during the twentieth century. They also found that the recent variations in the drought area closely relate to changes in ENSO frequency. Interannual variability of the summer precipitation regime over the United States, through modulation of the North American monsoon system, has been shown (Higgins et al. 1998, 1997) to be linked to the SSTs in the eastern Pacific and cold tongue regions, via anomalous Hadley circulation.

ENSO influence on wintertime intraseasonal extreme precipitation and temperature over the United States has been documented by Gershunov (1998) and Gershunov and Barnett (1998a). They find that the ENSO-based predictability of extreme rainfall and temperature is sensitive to the ENSO phase and is spatially variable. Furthermore, there is an asymmetric response of precipitation and temperature with respect to El Niño and La Niña phases. Model reproduction of these general features has been reported by Gershunov and Barnett (1998a). These observational and model findings have useful implications for long-range predictability.

It is not clear whether these changes are due to 1) variations in ENSO strength and frequency and the nonlinearity of the teleconnection; 2) extratropical decadal ocean–atmosphere variability, for example, the NAO (Hurrell and van Loon 1997; Kushnir 1994; Mann and Park 1996) and interdecadal variability, for example, the North Pacific Oscillation/Pacific Decadal Oscillation (PDO; Mantua et al. 1997; Gershunov and Barnett 1998b; Gershunov et al. 1999) modulating the ENSO response; or 3) secular changes related to century-scale global warming that may have changed the planetary climate dynamics. Relationships between decadal variations in ENSO, and the state of the PDO or NAO are also unclear at this point. Weaver (1999), Gu and Philander (1997), and Trenberth and Hurrell (1993) suggest that internal ENSO modulation and subsequent teleconnection to the North Pacific can explain the PDO. Latif and Barnett (1994) explain the interdecadal variability in the North Pacific through subtropical gyre mechanisms. In two recent papers, Barnett et al. (1999a,b) provide evidence of an ocean–atmosphere coupled mode in the Pacific midlatitude as the origin of decadal variability. They also suggest that decadal changes over the North Pacific can cause modulations of ENSO.

In the Atlantic, the nature of decadal variability of NAO is far from conclusive. Two hypotheses compete to explain this variability: coupled ocean–atmosphere and uncoupled modes of variability. In the coupled mode hypothesis, pronounced decadal changes in the SST and sea level pressure (SLP) in the subpolar and subtropic Atlantic gyres have been observed from data (Kushnir 1994; Deser and Blackmon 1993; Tourre et al. 1999), suggesting coupled ocean–atmosphere interactions. This is largely viewed as a low-frequency response of the ocean to atmospheric forcing (e.g., NAO), and its feedback on the atmosphere, resulting in oscillatory behavior. The uncoupled mode of variability is viewed as a passive response of the atmosphere to internally generated oceanic variations (Delworth et al. 1993; Barnett 1985; Grotzner et al. 1998), or as due to stratospheric cyclonic vortex (Kodera et al. 1996). Causes for variability on decadal to interdecadal timescales are areas of active research.

Droughts can have variable spatial scale depending on their severity and duration. Regional drought likely reflects a consistent response to large-scale climate patterns. There is considerable interest in the use of ENSO forecasts and teleconnections for seasonal to interannual forecasts of North American climate and, in particular, of regional summer droughts. In this context, it is necessary to develop a diagnostic understanding of how the preceding winter (and earlier) ENSO and, more generally, global SST states affect the spatial structure of summer drought. Given the ENSO perspective above, the variation in the relationship between winter ENSO or global SSTs and summer drought indices at interannual to interdecadal timescales is of particular interest. Should ENSO be considered as an episodic behavior of the climate system, with a typical episode life cycle of 12–18 months, or as a continuous phenomenon with a continuous hydrologic response? Is the information needed to predict continental drought response contained in measures of ENSO, or does one need extratropical SST information to properly resolve the winter climate–summer drought association? Insights into these issues are useful for selecting proper statistical prediction methods, as well as for making decisions concerning the specification of dynamic coupled ocean–atmosphere models used for seasonal to interannual drought forecasting.

In this paper, we explore these issues using century-long historical instrumental data on SST fields and the PDSI. The spatial and temporal variations in the teleconnection response of summer drought over the con-

tinental United States and the associated variations in winter SST fields are analyzed for three nonoverlapping, approximately 30-yr epochs of the twentieth century that have different ENSO, PDO and NAO attributes. The Niño-3 index is used for ENSO, and standard indices are used for the PDO and NAO, as described in the next section. Specifically, we assess, for the full record and for each of the three epochs, 1) the correlations between the PDSI and Niño-3, PDO and NAO indices; 2) the partial correlations between PDSI and one of the indices, given one of the other two indices; 3) the correlation between PDSI and Niño-3 for El Niño and La Niña years only; and 4) a singular valve decomposition (SVD) of the joint correlation structure of the continental PDSI and the global SST fields. These analyses are used to describe the space–time variation in the respective teleconnections, with a primary focus on ENSO, and for inferences on whether 1) the interdecadal changes in the teleconnections can be attributed directly to variations in ENSO, 2) the PDO and NAO contribute any linear information beyond that provided by Niño-3, and 3) the leading components of mutual correlation structure across the spatially distributed global winter SST and summer PDSI fields have coherent and consistent structure across the three epochs.

2. Data

The following data were used in our study:

1) global SST anomalies on a 5° × 5° grid from a ''reduced space'' optimal smoother algorithm applied to 131 years (1865–1995) of global SST monthly anomalies obtained from the U.K. Hadley Centre archives (Bottomley et al. 1990; Kaplan et al. 1998);
2) PDSI data on a 2° latitude × 3° longitude grid obtained from a nearest neighbor gridding procedure of Cook et al. (1999), applied to the Climate Division PDSIs from the National Climate Data Center for the period 1895–1995;
3) Niño-3 index, a widely used index of ENSO activity, obtained by averaging the SST anomalies [from the Kaplan et al. (1998) dataset] in the region comprising 5°S–5°N and 150°–90°W;
4) NAO index, defined as the difference in normalized SLP anomalies between Ponta Delgada (Azores) and Reykjavik (Iceland); and
5) PDO index, defined in Mantua et al. (1997).

We perform all the analyses for the common period of 1895–1995.

The PDSI, a measure of moisture deficit, takes into account both temperature and precipitation and also contains information from previous seasons (Palmer 1965). The PDSI is a standardized index that has comparable meaning at all locations. Negative values of the index imply droughtlike (or moisture deficit) conditions, and vice versa. Variants of the PDSI, such as the modified PDSI, and the hydrologic drought index emphasize different aspects of drought persistence. We do not discuss the merits of different indices here, and use only the PDSI, which is the most commonly cited index. The summer PDSI reflects a memory of the precipitation and temperature experienced at each location in, approximately, the previous 12-month period.

Winter SSTs are defined as the October–March averages of SST at each grid point. Summer PDSIs are the average of the June–August PDSI values. The Kaplan et al. (1998) SST dataset used by us reconstructs gridded SST values back to 1856, using ship track records and an optimal estimation procedure that relies on an empirical orthogonal function decomposition of the recent high quality records. From the estimated data covariance patterns, the method fills gaps, corrects sampling errors, and produces spatially and temporally coherent datasets. Cross-validated tests of their algorithm showed a high fidelity of the large-scale patterns inferred from sparse samples (similar to the pre-1930 data locations) to the observed patterns.

3. PDSI–Niño-3 teleconnections and extratropical factors

For simplicity, we chose to divide the period of record into three roughly equal epochs (1895–1928, 1929–62, and 1963–95) for analysis of time variations in the teleconnections. Moving window and wavelet analyses reveal changes in the frequency and amplitude of the key climate oscillations. Kestin et al. (1998) note that the dominant frequencies of ENSO do not seem to be constrained to a fixed frequency band, and that ENSO has been more active in approximately the 1960–99 and 1895–1920 periods than in the intervening period. Correspondingly, a number of continental hydrologic time series show a U-shaped trend over the twentieth century (Baldwin and Lall 1999; Lall and Mann 1995). The exact years at which trends in different indices change sign are not always consistent. Cole and Cook (1998) used 15-yr blocks to look at the correlation structure of the Southern Oscillation index with instrumental and tree-ring reconstructed PDSI. Their results are generally consistent with our analysis using Niño-3.

Figure 1 maps the correlations between the summer PDSI at each grid point over the United States and the preceding winter (December–January–February) Niño-3 value for the three epochs. Only correlations significant at the 95% level are shown. Since autocorrelation of Niño-3 is not significant, the standard significance test for the correlation of two series was used. We also checked the field significance, as suggested in Livezey and Chen (1983), and found that the correlations pass this test, as well, at a 99% significance level ($p < 10^{-8}$). Large regions of the United States exhibit spatially coherent correlations with Niño-3. However, the location and strength of these teleconnections varies by epoch. At the beginning of the century (Fig. 1a), a

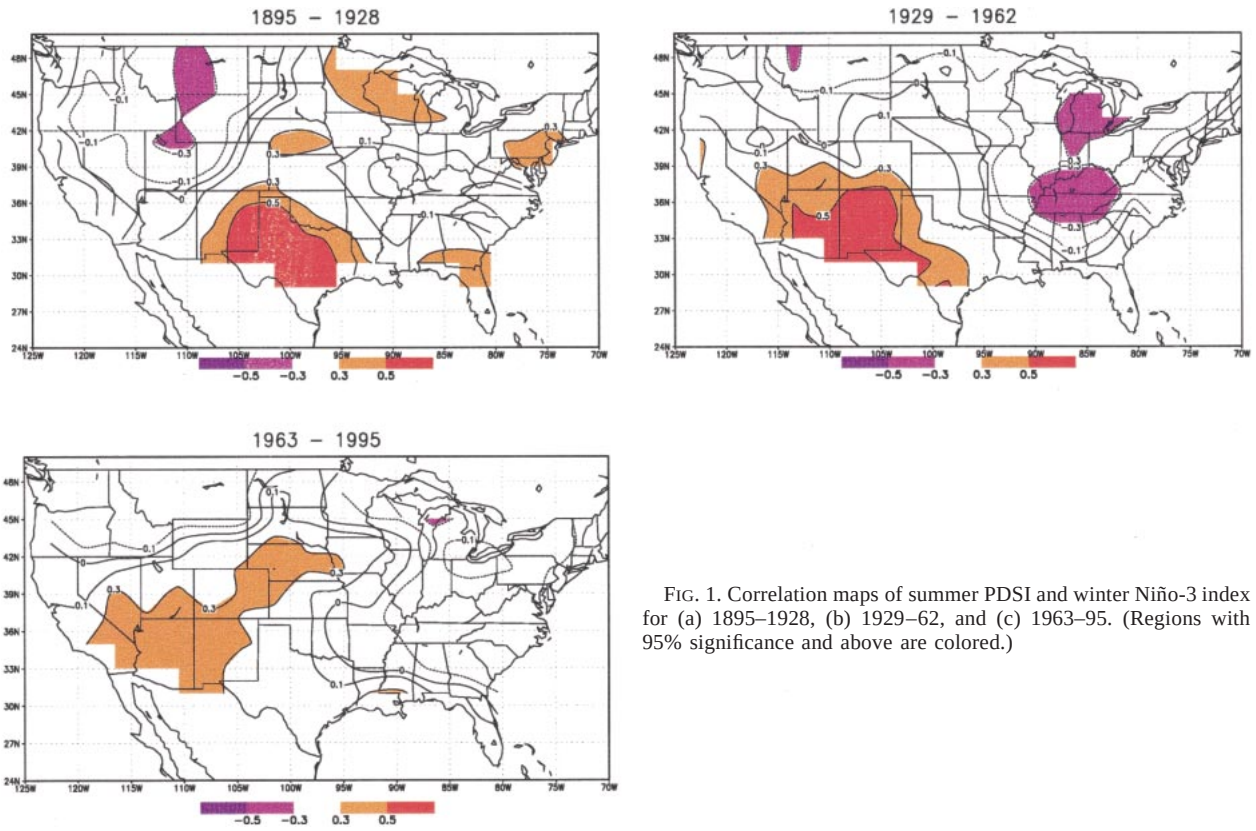

FIG. 1. Correlation maps of summer PDSI and winter Niño-3 index for (a) 1895–1928, (b) 1929–62, and (c) 1963–95. (Regions with 95% significance and above are colored.)

striking feature of the teleconnection is the strong positive correlation between PDSI and ENSO covering southeastern Texas, with weaker extensions into the Midwest, all the way to the Great Lakes region. There is also an area of negative correlation west of the Rockies. During the second epoch (Fig. 1b), the strong positive correlations have moved westward, covering southwestern Texas, as well as southern New Mexico and Arizona. The positive correlations in the Midwest that were observed in the first epoch are now absent. The Great Lakes and the east central regions are now negatively correlated. In the most recent epoch, 1963–95, the positive correlations are somewhat weaker and cover a more diffuse westward region, that is, southern California, Nevada, and Arizona, with extensions into the Midwest. Similar epochal variations in the ENSO teleconnections have been reported by Cole and Cook (1998) from instrumental and tree-ring reconstructed PDSI.

TABLE 1. ENSO years in the three epochs (El Niño years are in italics).

Epoch	ENSO years	No. of years
1895–28	*1897, 1900, 1903, 1905, 1906,* 1910, *1912, 1914, 1915, 1917, 1918, 1919, 1920, 1924, 1926*	16
1929–62	*1931, 1939, 1940, 1941, 1942,* 1943, 1950, 1956, *1958*	9
1963–95	*1966,* 1968, *1970, 1971, 1973,* 1974, 1976, *1977, 1983, 1987, 1988, 1989, 1992, 1995*	14

It is known that a few strong ENSO episodes can contribute to the observed correlations in the teleconnection response, and that the response can depend on the ENSO indicator. Could the change in the relative frequency and strength of El Niño/La Niña events be a leading factor in the explanation of the different spatial correlation structure for the three epochs? Conditional correlations between PDSI and Niño-3 for ENSO and non-ENSO events in each epoch were computed to address this question. ENSO events were classified as those having an absolute value of the winter Niño-3 index larger than 0.75 (this is roughly the 1σ level). The ENSO years in each epoch are identified in Table 1. The PDSI correlations with ENSO events are shown in Fig. 2. Again, only correlations significant at the 95% level are shown, accounting for the unequal sample sizes for each computation. In the first and third epochs, the correlation patterns for ENSO years (Figs. 2a,c) and all years in the epoch (Figs. 1a,c) are very similar. Note that the significance levels for correlation are substantially higher in Fig. 2, given the reduced sample sizes. The 1929–62 period shows no significant regions for correlations in ENSO years (Fig. 2b). An examination of all the correlations (not just the significant ones)

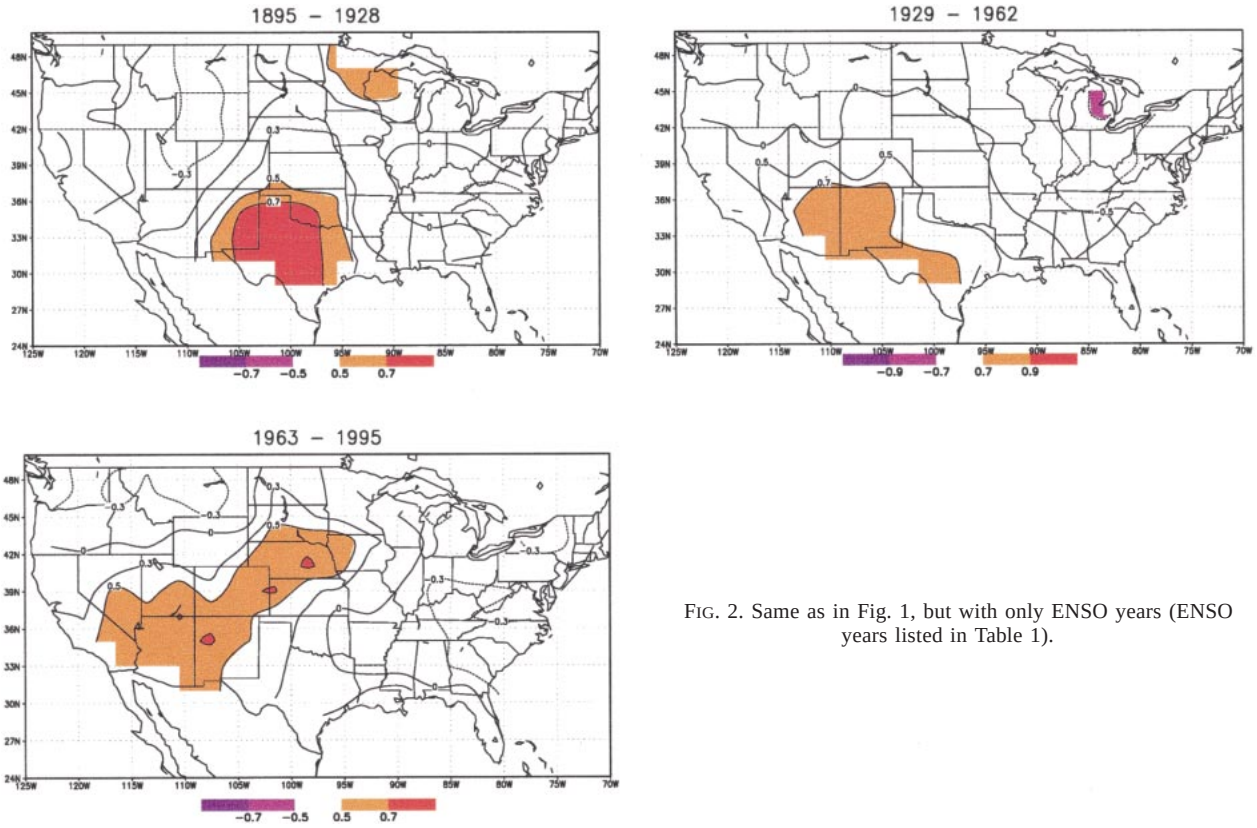

FIG. 2. Same as in Fig. 1, but with only ENSO years (ENSO years listed in Table 1).

shows that the spatial pattern of correlation is similar to that in Fig. 1b. The small sample size of ENSO years in this epoch and the associated higher significance levels lead to the apparently anomalous conclusion. Correlation patterns for non-ENSO years show no significant correlation in any of the epochs. This indicates that the teleconnection response in the summer PDSI is largely due to ENSO. We also computed correlations between PDSI and Niño-3 for years in which 1) Niño-3 > 1.25 (14 yr), 2) $1.25 >$ Niño-3 > 0.75 (12 yr), and 3) Niño-3 < -0.75 (13 yr). The statistically significant spatial correlation patterns for PDSI in each of these sets were essentially identical. We also did a *t* test for differences in the means of the PDSI responses for 26 El Niño (positive response) and 13 La Niña events (negative response). By changing the sign of the La Niña response, we are able to test for asymmetry in the El Niño–La Niña response. The *t* test was done allowing for unequal population for the two samples. The number of significant differences in conditional PDSI means at the 5% and 10% levels was consistent with what would be expected by chance. These results suggest that 1) the summer PDSI response to Niño-3 is essentially linear, 2) changing relative frequencies of ENSO events in an epoch can change the apparent correlation with PDSI, and 3) the spatial structure of the teleconnection does vary by epoch, due to either modulation by another variable or to changing ENSO strength and persistence.

The first observation is at odds with the observed response of winter precipitation and temperature to ENSO (see, for instance, Gershunov et al. 1999). Here, the difference is likely due to the time integrated nature of PDSI and potential changes in the season-by-season teleconnections to ENSO. It is also possible that the ENSO–PDSI relationship is nonlinear, but we are unable to detect it with the tools used. The second observation suggests that an approach that models ENSO as an episodic process (e.g., a marked nonhomogenous point process), or through a time–frequency decomposition (e.g., using wavelet methods), and models the PDSI teleconnection response through a nonlinear regression or transformation function may be useful. From a dynamical modeling perspective, the dynamical model would need to be able to generate the richness in ENSO variations seen in nature at interannual and interdecadal timescales, as well as the subsequent modulation of the teleconnections. The third observation deserves further attention. Gershunov et al. (1999) and Gershunov and Barnett (1998b) argue for the influence of the North Pacific variability in modulating ENSO–winter precipitation teleconnections. We explore the possibility of modulation of the ENSO–PDSI teleconnection by extratropical climate state through a partial correlation analysis with respect to the NAO and the PDO indices, which have a decadal to interdecadal character and may

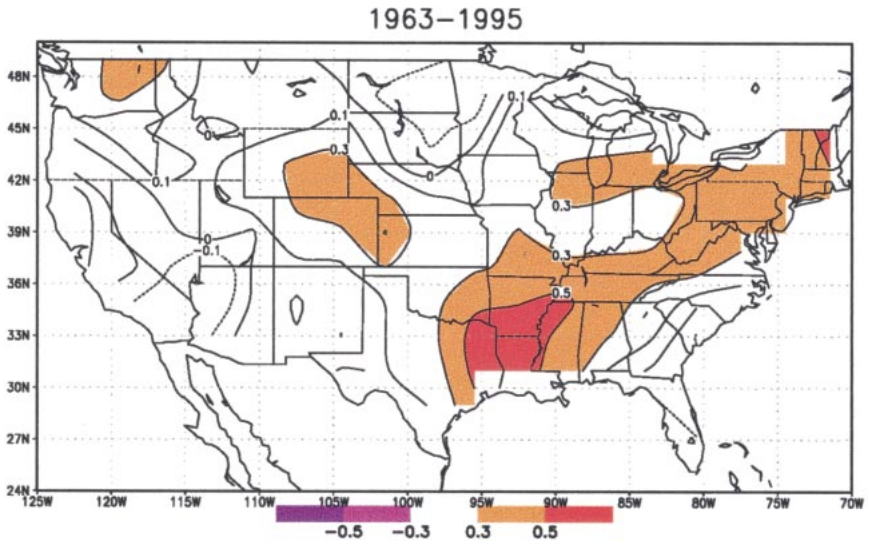

FIG. 3. Partial correlation maps of summer PDSI and winter NAO/Niño-3.

hence be relevant for explaining the interdecadal shifts in the teleconnection.

4. Partial correlation analyses

The NAO and the PDO indices are correlated with the Niño-3 index, so partial correlations for these variables are more useful than a direct comparison of correlation maps for each indicator. We looked at partial correlation maps of PDSI–Niño-3/NAO, PDSI–Niño-3/PDO, PDSI–PDO/Niño-3, and PDSI–NAO/Niño-3, for each epoch. The partial correlations are computed in the following manner. Consider the case of PDSI–Niño-3/NAO. We first perform a linear regression of PDSI on Niño-3. Residuals from the regression are then correlated with NAO (cf. Cole and Cook 1998, their Figs. 3b,c). Interestingly, the partial correlation maps for Niño-3, given either PDO or NAO, are essentially identical to Fig. 1, in which the direct Niño-3 correlation was computed. This suggests that knowledge of the extratropical indices does not change the ENSO teleconnection to PDSI. Next we consider the partial correlation of PDSI to PDO or NAO, given Niño-3. For the first two epochs, no significant correlations for large contiguous regions were found. Results for the third epoch are shown in Fig. 3. The spatial partial correlation pattern in Fig. 3 suggests that a large region, from eastern Texas to New England, and to the Great Lakes and the midwestern United States, is positively correlated with the NAO/Niño-3. This pattern is consistent with those found by Hartley and Robinson (1999) and Higgins et al. (1999) in their studies of variability of wintertime temperature and precipitation over the United States. A similar but more localized negative partial correlation pattern in the southeast United States is noted for PDSI–PDO/Niño-3. Our analysis of the PDO role on PDSI–Niño-3 connections is at odds with the PDO–Niño-3 winter precipitation results of Gershunov et al. (1999). This could be due to differences in the methods used and also to the nature of the target variables.

5. SST–PDSI connections

Having identified the epochal nature of the spatial teleconnection pattern of PDSI to ENSO and the two extratropical indices, we now investigate which regions of the global oceans participated in the PDSI teleconnection over the three epochs. The climate indices used are typically developed using limited areas of the ocean, and multivariate information about the joint state of the ocean evolution can be lost or confused in the process. It is also of interest to directly identify coherent spatial response regions for PDSI that relate to specific SST patterns. If this can be done reliably, a more parsimonious prediction scheme can be devised. To explore this issue, we perform a joint SVD of the winter SSTs and summer PDSIs at each grid point. The SVD analysis decomposes the covariance matrix of these two fields into orthogonal pairs of spatial patterns that maximize the squared temporal covariance between the two variables (Bretherton et al. 1992). The theory of SVD is discussed and compared with other multivariate techniques in Bretherton et al. (1992) and Wallace et al. (1992). The SVD of the covariance matrix of the PDSI and SST fields results in two matrices of singular vectors and one set of singular values. Each singular vector pair describes spatial patterns for each field, which have overall covariance given by the corresponding singular value. This is similar to canonical correlation analysis (CCA), in that both methods try to optimize joint patterns between the two fields. For in-depth analysis of CCA and its relation with SVD we refer the reader to Barnston and Smith (1996).

From the singular vector pairs, a so-called temporal

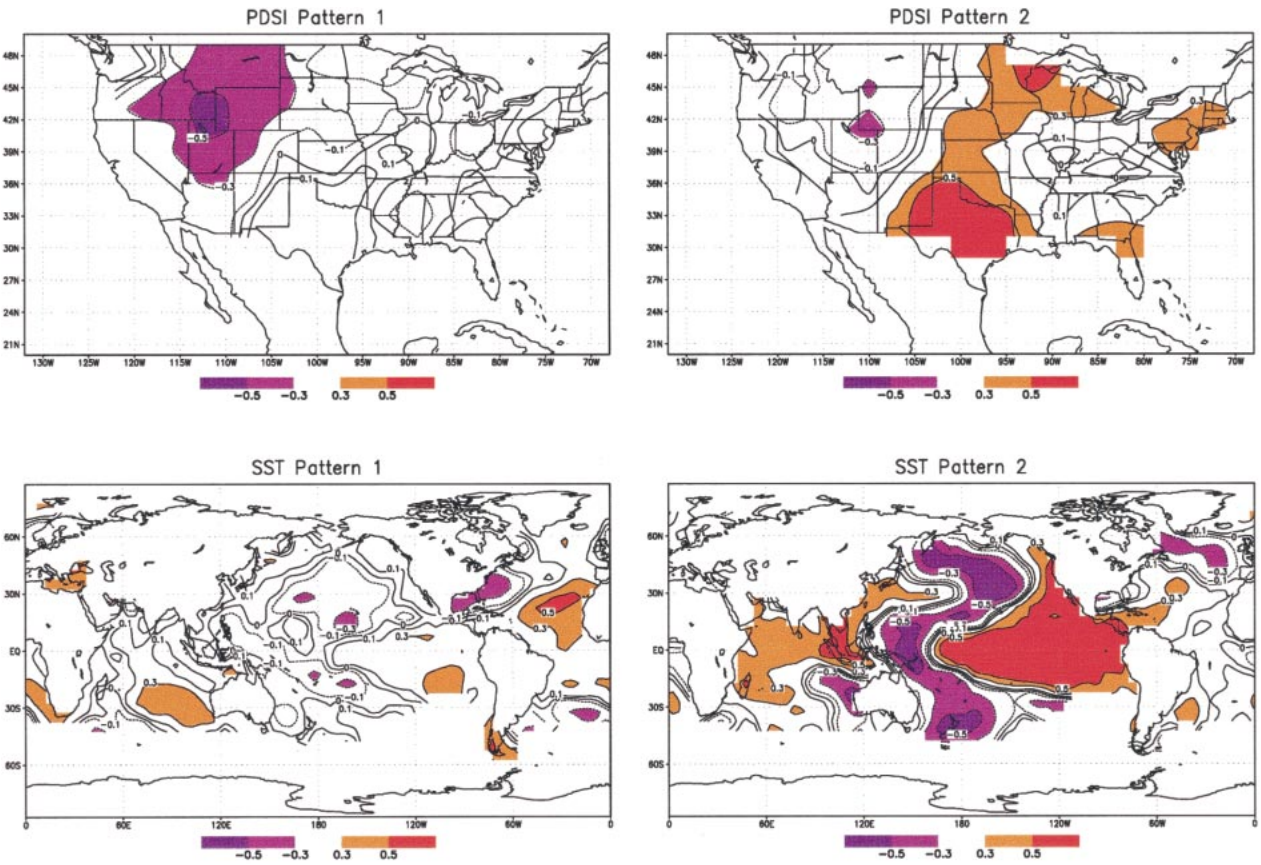

FIG. 4. Heterogeneous correlation map for SVD modes for PDSI (a) first mode and (b) second mode, and for global SSTs (c) first mode and (d) second mode, during the period 1895–1928.

expansion series (similar to a principal component series in EOF analysis) for each field can be obtained by projecting the data onto their corresponding singular vectors (Bretherton et al. 1992). The correlations between the values of each grid point of one field and the temporal expansion values of the other field result in heterogeneous correlation maps. In our application, the patterns shown by heterogeneous correlation maps for the *k*th SVD expansion mode indicate the strength of PDSI (SST) relative to the *k*th expansion coefficient of SST (PDSI). The different heterogeneous maps of each field are mutually orthogonal in the space domain.

Wallace et al. (1993) define a normalized squared covariance (NSC) value associated with each pair of spatial patterns, which indicates the strength of the relationship between the two fields. We use the NSC in the present study to compare the variability in SST and PDSI fields using a common scale.

We perform SVD analysis on the PDSI and SST data separately for the three epochs. The first two modes capture about 40%–50% of the joint variance in all three periods. The resulting heterogeneous correlation maps are shown in Figs. 4, 5, and 6.

a. The 1895–1928 period

Figure 4 shows the heterogeneous maps for the 1895–1928 period. In this and subsequent figures, correlations above 0.3 are statistically significant at the 95% level. In this period, the regions in the southern and eastern parts of Texas and regions of the Midwest extending up to the Great Lakes are strongly correlated with SSTs in the tropical Pacific and northern Pacific (Figs. 4b,d) in the second mode. This SST pattern is the widely known ENSO pattern, and the PDSI pattern is almost identical to the correlation pattern in Fig. 1 for the same period. This suggests that the spatial response of the PDSI is indeed due to ENSO. The pattern of the first mode is diffused, with no identifiable correlation regions for the SSTs. The PDSI shows a strong response in the Montana, Wyoming, and Utah regions. This suggests that the first pattern is predominantly a PDSI pattern with no coherent SST variability. The NSC value for the ENSO (second) pattern is 19%, while that for the first pattern is 25%.

b. The 1929–62 period

This period shows a weaker spatial extent of the ENSO pattern in the heterogeneous map (Fig. 5) com-

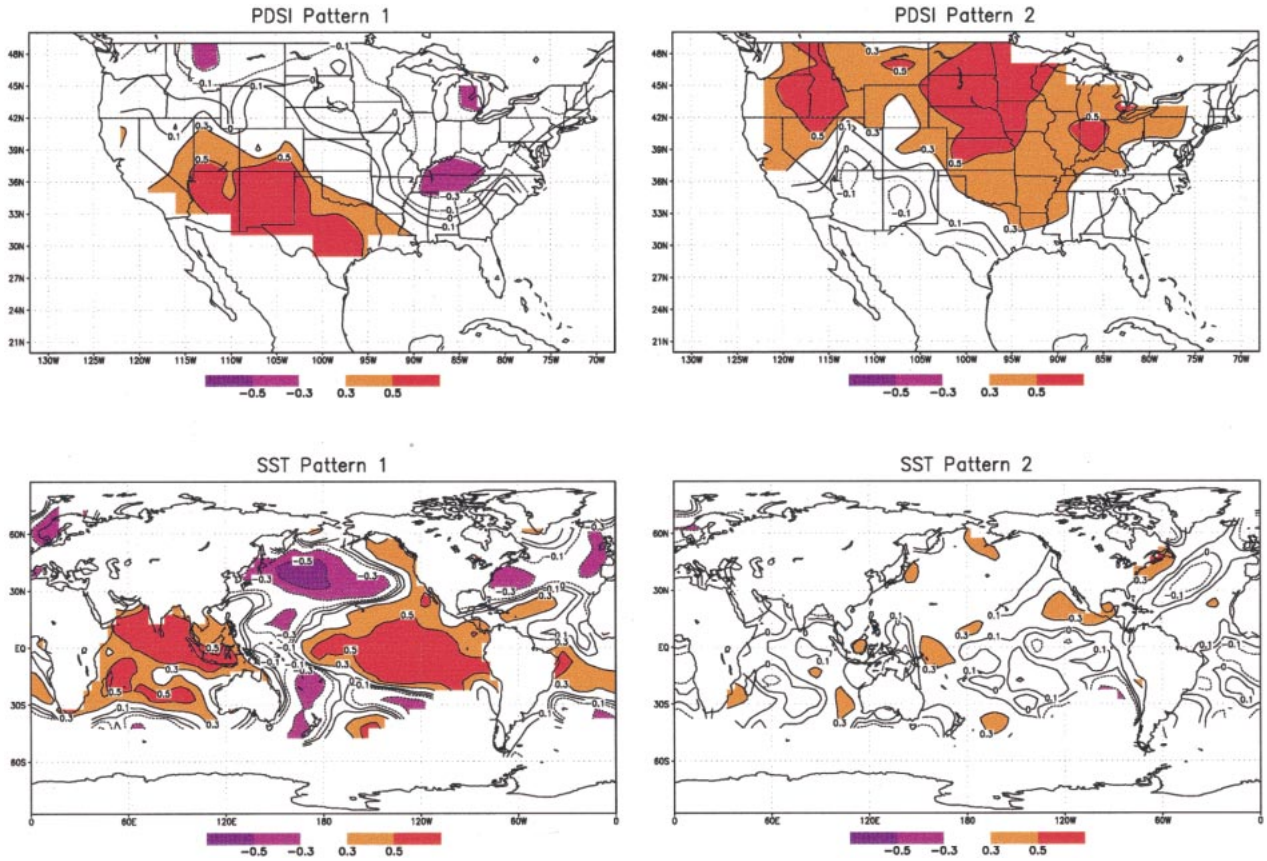

FIG. 5. Same as in Fig. 4, but for the period 1929–62.

pared to the previous period, consistent with the observation that ENSO activity was subdued in this epoch. Additionally, the strong negative correlation in the western Pacific region observed in the earlier period is absent here. The PDSI pattern corresponding to ENSO is spread out along southeastern Texas, southern New Mexico, and Arizona. The PDSI correlation extending into the Midwest that was seen in the earlier period is absent. In other words, the response is restricted to regions of the southwestern United States. The NSC value for this pattern is about 18%.

The map for the second mode, like that for the first mode in the earlier period, does not show a coherent SST pattern, while the PDSI exhibits a strong correlation covering almost the entire northern United States. This, again, indicates that the observed relationship is a PDSI-only mode, with no clear SST signal. This pattern has an NSC value of 12%. The NSC values of the two patterns are very similar, unlike for the previous period. The fact that ENSO was weaker in this period could be the reason that the variance is distributed similarly between the two modes.

c. The 1963–95 period

During the 1963–95 period, ENSO frequency and magnitude were high. This was also a period of increasing global surface temperatures. The heterogeneous correlation maps in the PDSI (Fig. 6) show a pattern covering southern California, Nevada, and Arizona, with projections into the Midwest. The associated pattern in the SSTs resembles an ENSO pattern, similar to that seen in the first period and to the Niño-3 correlations presented earlier. A significant difference is the sharp westward shift of the teleconnection response in the PDSIs relative to the first two periods. This has implications for statistical forecasting, because statistical models developed on the basis of teleconnection responses and SST indices for the earlier periods will be unsuccessful in this period. There are also subtle differences in the spatial structure of the tropical Pacific SST correlation pattern in this epoch. While it is not clear that the differences in the SST spatial patterns for the ENSO mode in the three epochs are statistically significant, they do provide some insights. The numerical modeling experiments of Hoerling et al. (1997) suggest that SST anomalies placed at different locations in the equatorial and tropical Pacific can lead to rather different spatial signatures and strengths for the continental precipitation and temperature teleconnections. In particular, the atmospheric moisture flow and tropical–extratropical teleconnection is influenced by the location of the primary tropical convection centers in the ENSO

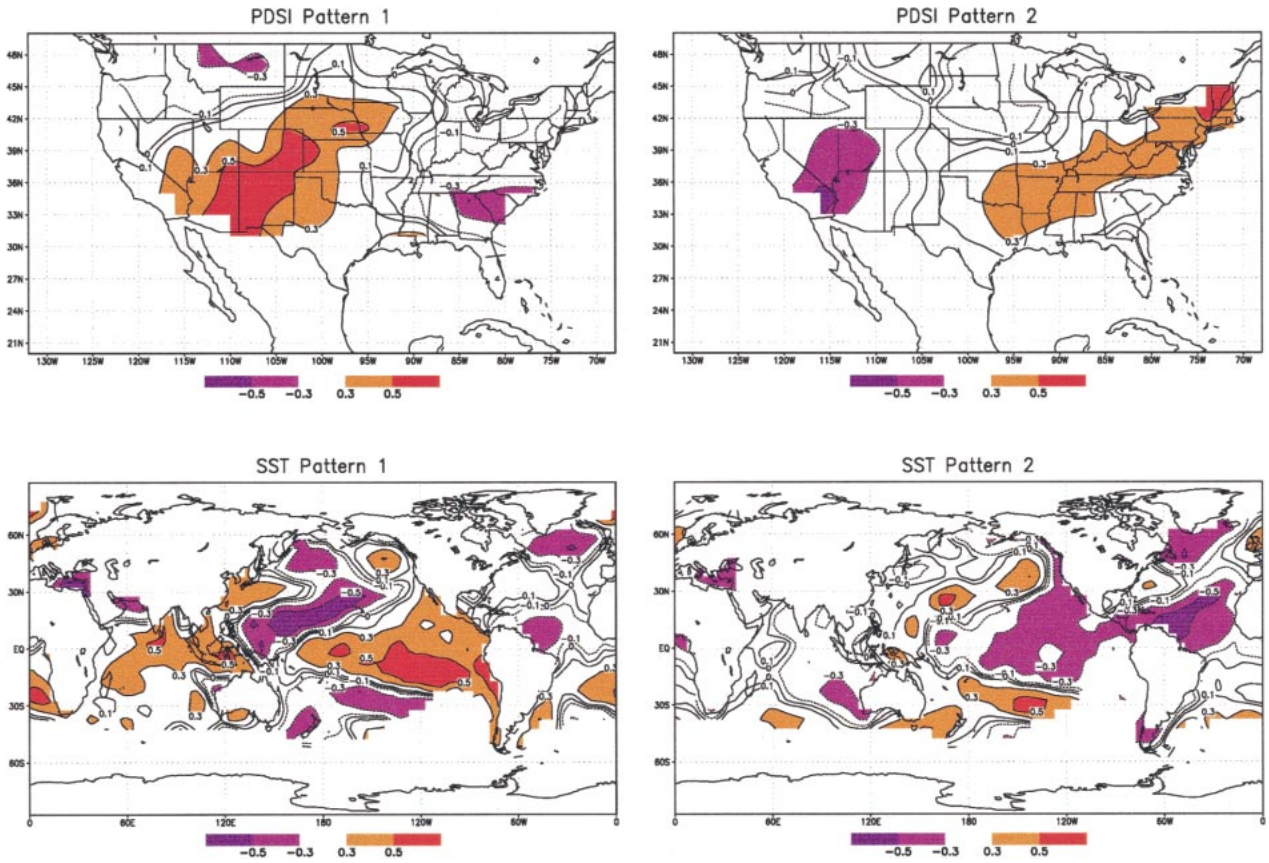

FIG. 6. Same as in Fig. 4, but for the period 1963–95.

region. There is evidence for changes in the spatial distribution of tropical convection associated with ENSO activity in recent decades (Krishna Kumar et al. 1999b). This might have a significant impact on the ENSO-related teleconnections to Northern Hemisphere climate variables.

Another significant feature is that of the second pattern. Here the SSTs exhibit a correlation structure in the Atlantic that resembles that of the SST pattern associated with the NAO (Deser and Blackmon 1993; Tourre et al. 1999). During this period, the NAO and the PDO have been anomalous, as indicated earlier. Note that the correlations with the SSTs in the North Pacific and in the equatorial Pacific reflect the key PDO centers (Mantua et al. 1997). The PDSI pattern in the correlation map associated with this SST pattern covers the region from the northeastern to the southeastern United States. This is much like the response we identified earlier from the partial correlation maps of PDSI with NAO and PDO given Niño-3 (Fig. 3) for this epoch and is different from what is observed in the previous epochs. Further, the correlation of the temporal expansion series of SST and PDSI of this mode with NAO time series (Hurrell 1995) is 0.4 and 0.5, respectively. The spatial pattern in the PDSI is similar and consistent with those from Hartley and Robinson (1999) and Higgins et al. (1999) that looked at wintertime temperatures over the United States and their links to SSTs. This analysis suggests that for this epoch the NAO–PDO–PDSI interaction may be captured in a single SST mode that is distinct from the ENSO–PDSI teleconnection mode.

d. Summary

The SST–PDSI correlation analysis across the three epochs was also repeated using correlation rather than covariance as the metric. The resulting spatial modes were essentially identical and are not reproduced here. The main difference in this analysis was that in epoch 1, the order of the two modes is switched, with the ENSO mode leading, consistent with the other two epochs. While the ENSO SST modes identified are spatially similar in the three epochs, they differ in their details. It is possible that the difference in the spatial pattern of PDSI correlation noted for these modes in the different epochs is due to these details and also to the differences in the spatial correlation structure relative to Niño-3 that was noted earlier. This relates to the common observation that each ENSO event is different in its manifestation in the SST field and its continental teleconnection [see, for instance, the discussion in Hoer-

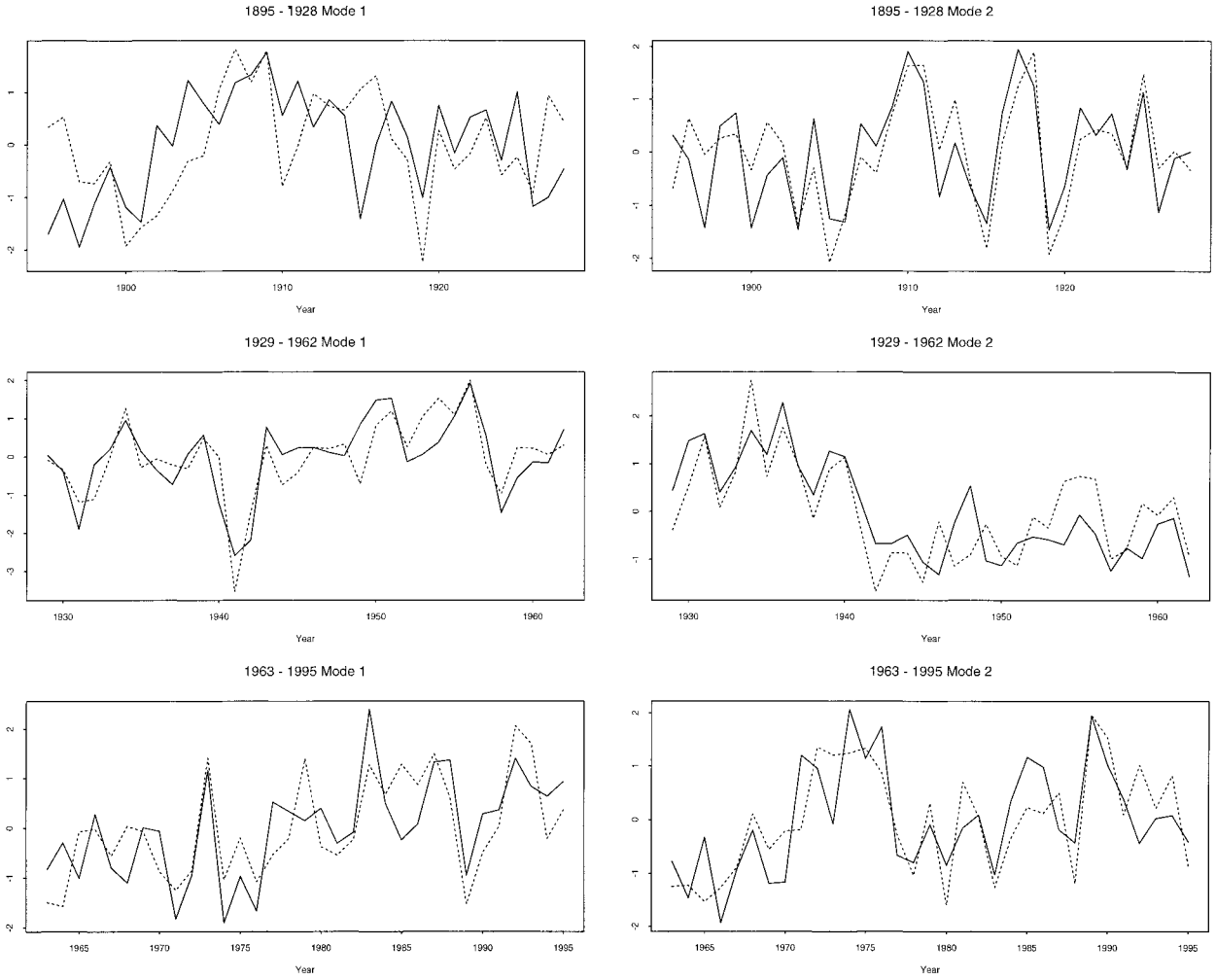

FIG. 7. Temporal expansion series of the first two modes in the three epochs. The solid lines represent the SST mode and the dashed lines represent the PDSI mode.

ling et al. (1997), which links changes in SST anomaly centers to winter precipitation teleconnections].

The temporal expansion series of the first two modes in the three epochs are shown in Fig. 7. The strong correlation between the ENSO mode SST principal component (PC) and the corresponding PDSI mode is noteworthy for each of the epochs. The SST ENSO mode seems to carry most of the PDO-like signal with it in our analysis (see Figs. 4d, 5c, and 6c). This is consistent with the earlier observation that PDO does not contribute significant additional linear information to the PDSI–Niño-3 relationship. In terms of linear analyses, the key story appears to be the role of ENSO in all three epochs as a modulator of drought, with the North Atlantic playing a role in the eastern United States in the third epoch.

6. Conclusions and future directions

We have explored the relationships between low-frequency winter climate indicators and summer drought in the continental United States, with a view to developing a statistical forecasting scheme. Relatively robust teleconnections between ENSO and drought indices in the southwestern United States were established. However, the strength and spatial signature of the correlation fields was found to vary over time. The analysis suggests that the Niño-3–PDSI relationships are likely to be nonlinear and are determined primarily by ENSO events that exceed some Niño-3 threshold. Thus, a composite, categorical probability forecast may be more useful than a linear regression approach for one-season-ahead forecasting, and a more complex approach may be necessary for analyzing longer run structure. The need to better understand the spatial structure of the tropical Pacific and the global SST fields in predicting PDSI was highlighted. Details of both fields and their timescales of evolution are likely to be important for successful forecasting schemes.

The epochal variations in the teleconnections and the PDSI predictors suggest that naïve statistical forecasting

algorithms that use the full record may have limited predictability in practice. A Bayesian time series approach (West and Harrison 1997) that deals explicitly with nonstationarity, in the framework of dynamic linear models, may be more useful. Approaches based on wavelet decompositions may also be useful for such data. We plan to explore both methods in our future work. However, a more important problem concerns developing an understanding of why the nonstationarity occurs in the first place. Is it part of the nonlinear dynamics of the coupled system, or are we observing weakly coupled modes of the climate system that randomly evolve or are forced (e.g., by CO_2 changes) to a particular state? Empirical and conceptual approaches for insights into such questions need to be developed.

The PDSI and related variables are interesting in their own right when correlations with climatic predictors are sought. Like stream flow and lake volumes, the PDSI can reflect a relatively long-term memory modulated by seasonal factors. The frequency structure of such variables is a linearly or nonlinearly modulated version of the climatic forcing. The time integration associated with such a process can integrate over interseasonal climate structure, such as the negative correlation between winter snow and summer rainfall in the southwestern United States noted by Gutzler and Preston (1997). It is not always clear whether such seasonal averaging enhances or destroys predictability. We plan to explore the role of ENSO and the annual cycle in lending predictability to summer PDSI, as a function of the operative hydroclimatic mechanisms in different regions of the country. Both empirical analyses and conceptual modeling will be necessary to explore this multiscale interaction problem.

Acknowledgments. This work was supported by NOAA Grant NA76GP0416. We thank Yochanan Kushnir and Shaleen Jain for useful discussions. We are grateful to the two anonymous reviewers for their detailed comments and suggestions that helped improve the manuscript.

REFERENCES

Baldwin, C. K., and U. Lall, 1999: Seasonality of streamflow: The upper Mississippi River. *Water Resour. Res.,* **35,** 1143–1154.

Barnett, T. P., 1985: Variations in near-global sea level pressure. *J. Atmos. Sci.,* **42,** 478–501.

——, D. Pierce, M. Latif, D. Dommenget, and R. Saravanan, 1999a: Interdecadal interactions between the tropics and midlatitudes in the Pacific basin. *Geophys. Res. Lett.,* **26,** 615–618.

——, ——, R. Saravanan, N. Schneider, D. Dommenget, and M. Latif, 1999b: Origins of the midlatitude Pacific decadal variability. *Geophys. Res. Lett.,* **26,** 1453–1456.

Barnston, A. G., and T. M. Smith, 1996: Specification and prediction of global surface temperature and precipitation from global SST using CCA. *J. Climate,* **9,** 2660–2697.

Battisti, D. S., and E. S. Sarachik, 1995: Understanding and predicting ENSO. *Rev. Geophys.,* **33** (Suppl.), 1367–1376.

Bottomley, M., C. K. Folland, J. Hsiung, R. E. Newell, and D. E. Parker, 1990: *Global Ocean Surface Temperature Atlas.* HMSO, 20 pp. and 314 plates.

Bretherton, C. S., C. Smith, and J. M. Wallace, 1992: An intercomparison of methods for finding coupled patterns in climate data. *J. Climate,* **5,** 541–560.

Cane, M. A., S. E. Zebiak, and Y. Xue, 1995: Model studies of the long-term behavior of ENSO. *Natural Climate Variability on Decade-to-Century Time Scales,* D. G. Martinson et al., Eds., National Academy Press, 442–457.

Cayan, D. R., M. D. Dettinger, and N. E. Graham, 1998: Decadal variability of precipitation over western North America. *J. Climate,* **11,** 3148–3166.

Cole, J., and E. Cook, 1998: The changing relationship between ENSO variability and moisture balance in the continental United States. *Geophys. Res. Lett.,* **25,** 4529–4532.

Cook, E. R., D. M. Meko, D. W. Stahle, and M. K. Cleaveland, 1999: Drought reconstructions for the continental United States. *J. Climate,* **12,** 1145–1162.

Dai, A., K. E. Trenberth, and T. R. Karl, 1998: Global variations in droughts and wet spells: 1900–1995. *Geophys. Res. Lett.,* **25,** 3367–3370.

Delworth, T. L., S. Manabe, and R. J. Stouffer, 1993: Interdecadal variations of the thermohaline circulation in a coupled ocean–atmosphere model. *J. Climate,* **6,** 1993–2011.

Deser, C., and M. Blackmon, 1993: Surface climate variations over the North Atlantic Ocean during winter: 1900–1989. *J. Climate,* **6,** 1743–1753.

Dettinger, M. D., M. Ghil, and C. L. Keppenne, 1995: Interannual and interdecadal variability in United States surface–air temperatures, 1910–87. *Climatic Change,* **31,** 35–66.

——, D. R. Cayan, and D. V. Meko, 1998: North–south precipitation patterns in western North America on interannual-to-decadal timescales. *J. Climate,* **11,** 3095–3111.

Gershunov, A., 1998: ENSO influence on intraseasonal extreme rainfall and temperature frequencies in the contiguous United States: Implications for long-range predictability. *J. Climate,* **11,** 3192–3203.

——, and T. P. Barnett, 1998a: ENSO influence on intraseasonal extreme rainfall and temperature frequencies in the contiguous United States: Observation and model results. *J. Climate,* **11,** 1575–1586.

——, and ——, 1998b: Interdecadal modulation of ENSO teleconnections. *Bull. Amer. Meteor. Soc.,* **79,** 2715–2725.

——, ——, and D. Cayan, 1999: North Pacific interdecadal oscillation seen as factor in ENSO-related North American climate anomalies. *Eos, Trans. Amer. Geophys. Union,* **80,** 25–30.

Grotzner, A., M. Latif, and T. P. Barnett, 1998: A decadal cycle in the North Atlantic as simulated by the ECHO coupled GCM. *J. Climate,* **11,** 831–847.

Gu, D., and S. G. H. Philander, 1997: Interdecadal climate fluctuations that depend on exchanges between the tropics and extratropics. *Science,* **275,** 805–807.

Gutzler, D. S., and J. W. Preston, 1997: Evidence for a relationship between spring snow cover in North America and summer rainfall in New Mexico. *Geophys. Res. Lett.,* **24,** 2207–2210.

Halpert, M. S., and C. F. Ropelewski, 1992: Surface temperature patterns associated with the Southern Oscillation. *J. Climate,* **5,** 577–593.

Hartley, S., and D. Robinson, 1999: Atlantic sea surface temperatures and eastern United States climate, 1950–1992. Preprints, *Eighth Conf. on Climate Variations,* Denver, CO, Amer. Meteor. Soc., 94–97.

Higgins, R. W., J. E. Janowiak, and X. Wang, 1997: Influence of the North American monsoon system on the U.S. summer precipitation regime. *J. Climate,* **10,** 2600–2622.

——, K. C. Mo, and Y. Yao, 1998: Interannual variability of the U.S. summer precipitation regime with emphasis on the southwestern monsoon. *J. Climate,* **11,** 2582–2605.

——, A. Leetmaa, Y. Xue, and A. Barnston, 1999: Dominant factors influencing the seasonal predictability of United States precip-

itation and surface air temperature. Preprints, *Eighth Conf. on Climate Variations*, Denver, CO, Amer. Meteor. Soc., 98–103.
Hoerling, M. P., and A. Kumar, 1997: Origins of extreme climate states during the 1982–83 ENSO winter. *J. Climate,* **10,** 2859–2870.
——, ——, and M. Zhong, 1997: El Niño, La Niña, and the nonlinearity of their teleconnections. *J. Climate,* **10,** 1769–1786.
Hurrell, J., 1995: Decadal trends in the North American oscillation regional temperatures and precipitation. *Science,* **269,** 676–679.
——, and H. van Loon, 1997: Decadal variations in climate associated with North Atlantic oscillations. *Climatic Change,* **36,** 301–326.
Kaplan, A., M. A. Cane, Y. Kushnir, A. C. Clement, M. B. Blumenthal, and B. Rajagopalan, 1998: Analyses of global sea surface temperature 1856–1991. *J. Geophys. Res.,* **103,** 18 567–18 589.
Kestin, T. S., D. J. Karoly, J. Yano, and N. A. Rayner, 1998: Time–frequency variability of ENSO and stochastic simulations. *J. Climate,* **11,** 2258–2272.
Kiladis, G. N., and H. F. Diaz, 1989: Global climate anomalies associated with extremes in the Southern Oscillation. *J. Climate,* **2,** 1069–1090.
Kodera, K., M. Chiba, H. Koide, A. Kitoh, and Y. Nikaidi, 1996: Interannual variability of winter stratosphere and troposphere in the Northern Hemisphere. *J. Meteor. Soc. Japan,* **74,** 365–382.
Krishna Kumar, K., R. Kleeman, M. A. Cane, and B. Rajagopalan, 1999a: Epochal changes in Indian monsoon–ENSO precursors. *Geophys. Res. Lett.,* **26,** 75–78.
——, B. Rajagopalan, and M. A. Cane, 1999b: On the weakening relationship between the Indian monsoon and ENSO. *Science,* **284,** 2156–2159.
Kushnir, Y., 1994: Interdecadal variations in North Atlantic sea surface temperature and associated atmospheric conditions. *J. Climate,* **7,** 142–147.
Lall, U., and M. Mann, 1995: The Great Salt Lake: A barometer of interannual climatic variability. *Water Resour. Res.,* **35,** 1143–1154.
Latif, M., and T. P. Barnett, 1994: Causes of decadal climate variability over the North Pacific and North America. *Science,* **266,** 634–637.
Livezey, R. E., and W. Y. Chen, 1983: Statistical field significance and its determination by Monte Carlo techniques. *Mon. Wea. Rev.,* **111,** 46–59.
Mann, M. E., and J. Park, 1996: Joint spatiotemporal modes of surface temperature and sea level pressure variability in the Northern Hemisphere during the last century. *J. Climate,* **9,** 2137–2162.
Mantua, N. J., S. R. Hare, Y. Zhang, J. M. Wallace, and R. C. Francis, 1997: A Pacific interdecadal climate oscillation with impacts on salmon production. *Bull. Amer. Meteor. Soc.,* **78,** 1069–1079.
McCabe, G. J., and M. D. Dettinger, 1998: Decadal variability in the strength of ENSO teleconnections with precipitation in the western United States. *Int. J. Climatol.,* **19,** 1399–1410.
Palmer, W. C., 1965: Meteorological drought. Weather Bureau Research Paper 45, 1–58. [Available from U.S. Dept. of Commerce, Washington, DC 20044.]
Piechota, T. C., and J. A. Dracup, 1996: Drought and regional hydrologic variation in the United States: Associations with the El Niño–Southern Oscillation. *Water Resour. Res.,* **32,** 1359–1370.
Power, S., T. Casey, C. Folland, A. Colman, and V. Mehta, 1999: Inter-decadal modulation of the impact of ENSO on Australia. *Climate Dyn.,* **15,** 319–324.
Price, C., L. Stone, A. Huppert, B. Rajagopalan, and P. Alpert, 1998: A possible link between El Niño and precipitation in Israel. *Geophys. Res. Lett.,* **25,** 3963–3966.
Rajagopalan, B., U. Lall, and M. A. Cane, 1997: Anomalous ENSO occurrences: An alternate view. *J. Climate,* **10,** 2351–2357.
Riebsame, W. E., S. A. Changnon, and T. R. Karl, 1991: *Drought and Natural Resources Management in the United States: Impacts and Implications of the 1987–89 Drought.* Westview Press, 174 pp.
Rodo, X., E. Baert, and F. A. Comin, 1997: Variations in seasonal rainfall in southern Europe during the present century: Relationships with the North Atlantic oscillation and the El Niño–Southern Oscillation. *Climate Dyn.,* **13,** 275–285.
Ropelewski, C. F., and M. S. Halpert, 1986: North American precipitation and temperature patterns associated with the El Niño/Southern Oscillation. *Mon. Wea. Rev.,* **114,** 2352–2362.
——, and ——, 1989: Precipitation patterns associated with the high index phase of the Southern Oscillation. *J. Climate,* **2,** 268–284.
Tourre, Y., B. Rajagopalan, and Y. Kushnir, 1999: Dominant patterns of climate variability in the Atlantic Ocean region during the last 136 years. *J. Climate,* **12,** 2285–2299.
Trenberth, K. E., and G. W. Branstator, 1992: Issues in establishing causes of the 1988 drought over North America. *J. Climate,* **5,** 159–172.
——, and J. W. Hurrell, 1993: Decadal atmosphere–ocean variations in the Pacific. *Climate Dyn.,* **9,** 303–319.
——, and T. J. Hoar, 1996: The 1990–1995 El Niño–Southern Oscillation event: Longest on record. *Geophys. Res. Lett.,* **23,** 57–60.
——, and ——, 1997: El Niño and climate change. *Geophys. Res. Lett.,* **24,** 3057–3060.
Wallace, J. M., D. S. Gutzler, and C. S. Bretherton, 1992: Singular value decomposition of wintertime sea surface temperature and 500-mb height anomalies. *J. Climate,* **5,** 561–576.
——, Y. Zhang, and K.-H. Lau, 1993: Structure and seasonality of interannual and interdecadal variability of the geopotential height and temperature fields in the Northern Hemisphere troposphere. *J. Climate,* **6,** 2063–2082.
Weaver, A. J., 1999: Extratropical subduction and decadal modulation of El Niño. *Geophys. Res. Lett.,* **26,** 743–746.
West, M., and P. J. Harrison, 1997: *Bayesian Forecasting and Dynamic Models.* 2d ed. Springer-Verlag, 680 pp.